International Journal of Computational and Experimental Science and ENgineering
(IJCESEN)

Vol. 10-No.4 (2024) pp. 1735-1742
http://www.ijcesen.com

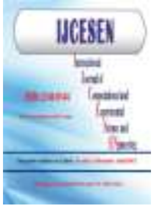

ISSN: 2149-9144

Research Article

Investigation of Epitaxial Misfit Strain Influence at the $CsSn(I_{1-x}Br_x)_3/SnO_2$ Interface on Photovoltaic Parameters in $Cu_2O/CsSn(I_{1-x}Br_x)_3/SnO_2$ Perovskite Solar Cells

Hayat ARBOUZ*

University Saad Dahlab Blida1, Faculty of Sciences, Department of Physics, 09000, Blida-Algeria
* **Corresponding Author Email:** arbouzhayet@yahoo.fr - **ORCID:** 0000-0003-2780-5215

Article Info:

DOI: 10.22399/ijcesen.367
Received : 01 July 2024
Accepted : 25 December 2024

Keywords :

Perovskite,
Solar Cell,
Strain,
Photovoltaic,
Efficiency.

Abstract:

This work involves the numerical simulation of the photovoltaic performance of a single perovskite solar cell based on the $Cu_2O/CsSn(I_{1-x}Br_x)_3/SnO_2$ structure, utilizing a lead-free inorganic perovskite absorber layer $CsSn(I_{1-x}Br_x)_3$ with variable bromine content represented by the ratio x. The study aims to evaluate performance fluctuations due to misfit deformation effects at the interface between the SnO_2 electron transport layer (ETL) and the absorber on photovoltaic parameters. The simulation model incorporates variations in the physical parameters of the device layers dependent on the ratio x. This enables the calculation of bandgap energy fluctuations according to strain theory and assesses the resultant impact on photovoltaic parameters due to strain at the $SnO_2/CsSn(I_{1-x}Br_x)_3$ interface. Performance results are presented as a function of bromine composition x, considering both the presence and absence of deformation effects. The study clearly demonstrates the significant impact of misfit deformation on bandgap energy fluctuation, emphasizing the need to optimize bromine content to balance deformation effects and achieve optimal performance. Specifically, the results show a maximum efficiency of 19.72% at x=0.56 for the undeformed structure, and 19.30% at x=0.50 for the deformed structure. This study refines simulation results and underscores the critical role of deformation engineering in modulating energy gaps.

1. Introduction

Remarkable progress in photovoltaic technology over recent decades has enabled the development of a wide range of high-performance conversion systems [1]. Various technologies in this field, from the oldest to the most recent, have all benefited from advances in scientific research, including experimentation, manufacturing, simulation [2], and the development of new materials [3]. Systems based on organic-inorganic perovskite materials like $MAPbI_3$ and $FAPbI_3$ have revolutionized photovoltaic conversion [4], showcasing rapid development and achieving competitive efficiencies that have quickly approached those of long-dominant silicon technology. Significant research efforts have been dedicated to developing solar cells based on perovskite absorbers, leading to efficiency improvements from 3.9% to 25.5% within a short timeframe [5], with the latest record at 26.8% [6]. However, concerns about the toxicity and instability of perovskites have prompted studies into lead-free and inorganic alternatives [7-10]. While numerous studies have explored the optical and electronic properties of perovskite thin films and solar cells across various compositions [11], little attention has been given to the physical deformations occurring during the epitaxial deposition of the absorber layer and their implications on electronic properties, such as bandgap energy, which are crucial for device performance. This study focuses on a single solar cell structure utilizing a lead-free, inorganic perovskite absorber, $CsSn(I_{1-x}Br_x)_3$, where x represents varying bromine content. Cu_2O and SnO_2 were chosen as hole transport layer (HTL) and electron transport layer (ETL) materials, t the respectively, consistent with prior research [12-13]. Photovoltaic performance was evaluated as a function of x using a detailed model that accounts for variations in the physical parameters of the absorber with bromine content. The impact of misfit strain a $CsSn(I_{1-x}Br_x)_3/SnO_2$ interface during epitaxial growth on the properties of the ETL layer was considered. The fluctuation in the absorber bandgap energy due to this strain and its influence on device performance were assessed using deformation theory. Results for the strained structure, accounting for misfit strain at the interface, were compared with those for the unstrained structure, which neglects such effects, to confirm bandgap energy fluctuations and emphasize the need for precise adjustment, which is crucial for optimizing photovoltaic parameters.

2. Device Architecture and Simulation Model

Figure 1 (a) shows the structure of the device studied, which concerns a single solar cell based on the perovskite absorber material $CsSn(I_{1-x}Br_x)_3$ with a composition that varies with the bromine content, in addition to being ecological due to the absence of lead and inorganic because it contains Cs instead of MA as in its $MAPbI_3$ counterpart, so that it shows better stability.

The structure follows the configuration Au / Cu_2O / $CsSn(I_{1-x}Br_x)_3$ / SnO_2 / FTO. The FTO was used as a transparent layer that facilitates the extraction of electrons from the junction, with a work function of 4.1 eV. Based on our research and previous work, the thickness of this layer was set at 200 nm. The Cu_2O and SnO_2 layers that surround the absorber layer are hole and electron transport layers HTL and ETL that play an important role in the optimal operation of the device [14]. These layers must be selected with particular care because their physical properties must satisfy their transport role and also help to maintain favorable surface conditions and appropriate energy barriers as shown in figure 1 (b), their thicknesses were optimized in our previous work and set at 100nm and 50nm respectively.

Increasing the bromine content in the absorber composition alters several physical properties of the material, including the bandgap energy. The bandgap energy ranges from 1.3 eV, corresponding to the pure iodine component, to 1.75 eV, corresponding to the pure bromine component. This variation is represented by equation 1, where the bromine content is denoted by the fraction (x).

The following equations represent the variation of key parameters: electron affinity, dielectric constant, acceptor density, defect density, and lattice parameter.

$$E_g(x) = 1.3(1-x) + 1.75x - 0.3x(1-x) \quad (1)$$

$$\chi(x) = 4.38(1-x) + 4.07x - 0.29x(1-x) \quad (2)$$

$$\varepsilon_r(x) = 9.93(1-x) + 6.76x \quad (3)$$

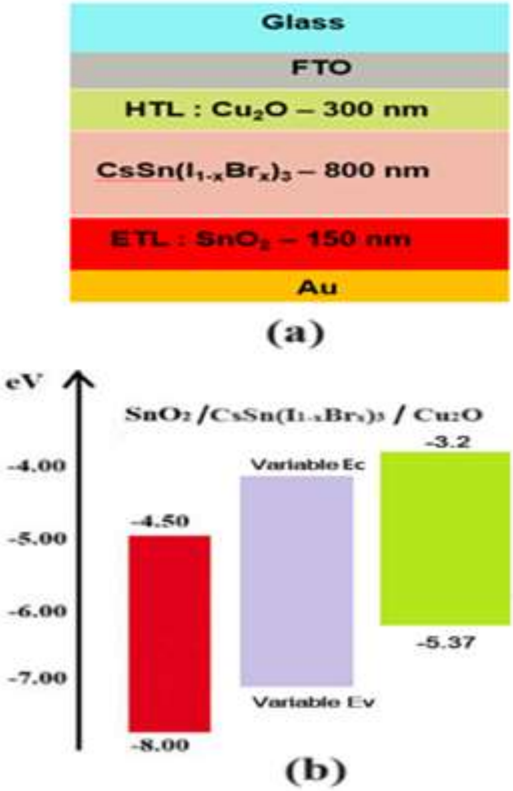

Figure 1. (a) *Schematic representation of the structure.* **(b)** *Energy Band Structure.*

$$N_a(x) = 10^{18}(1-x) + 10^{16}x \quad (4)$$

$$N_t(x) = 10^{15}(1-x) + 10^{16}x \quad (5)$$

$$a(x) = 6.292(1-x) + 5.901x \quad (6)$$

The photocurrent density is dependent on the solar spectrum F(λ) and the external quantum efficiency EQE(λ) as described by equation 7.

$$J_{ph} = q\int_{\lambda_{min}}^{\lambda_{max}} F(\lambda).EQE(\lambda)\, d\lambda \quad (7)$$

In this context, q denotes the elementary charge of an electron, F(λ) represents the wavelength-dependent solar irradiance spectrum, and λ_{min} and λ_{max} are the minimum and maximum wavelengths, respectively.

The current-voltage characteristic [15] has been calculated using equation 8.

$$J = J_{ph} - (J_0 + J_s).\left(e^{\frac{q.(V-JR_S)}{2kT}} - 1\right) - \frac{V-J.R_s}{R_{sh}} \quad (8)$$

Where J_0 is the recombination reverse dark current density, which depends on density of carriers, and lifetimes and diffusion coefficients.

$$J_0 = q.\left(\frac{\sqrt{D_p}}{\sqrt{\tau_p}}.\frac{n_i^2}{N_D} + \frac{\sqrt{D_n}}{\sqrt{\tau_n}}.\frac{n_i^2}{N_A}\right) \quad (9)$$

J_s represents the recombination current density at the interface [16], which is related to the carrier recombination rate at the interface as well as the shifts in the conduction and valence bands, ΔE_c and ΔE_v, respectively, as described below [17].

$$\Delta E_c = \chi_{ETL} - \chi_{PVK} \quad (10)$$

$$\Delta E_v = (\chi_{HTL} + Eg_{HTL}) - (\chi_{PVK} + Eg_{PVK}) \quad (11)$$

The photovoltaic parameters are calculated using formulas that are widely employed in the literature. These parameters include the efficiency, which is expressed by equation 12.

$$\eta = \frac{J_{sc}.V_{oc}}{P_i} \quad (12)$$

J_{sc} and V_{oc} represent the short-circuit current density and open-circuit voltage, respectively. In this study, we investigate the impact of the biaxial strain generated at the interface between the electron transport layer ETL material and the perovskite absorber, on the device performance. The misfit strain considered arises from the difference in lattice parameters between the $CsSn(I_{1-x}Br_x)_3$ perovskite absorber and the SnO_2 ETL in the epitaxial direction. This strain is described by the following relationship [18]:

$$\varepsilon = \varepsilon_{xx} = \varepsilon_{yy} = \frac{a_{PVK} - a_{ETL}}{a_{ETL}} \quad (13)$$

a_{ETL} and a_{PVK} represent the lattice constants of ETL and perovskite absorber respectively.

In the z-oriented axis, the strain is expressed as:

$$\varepsilon_{zz} = -2\frac{C_{12}}{C_{11}}.\varepsilon \quad (14)$$

C_{11} and C_{12} are the elastic stiffness constants of the strained layer. According to strain theory [19], the misfit strain induces fluctuations in the energy band edges, which in turn modify the bandgap energy of the absorber. The shift in the conduction band edge is given by:

$$\delta E_c = a_c.(\varepsilon_{xx} + \varepsilon_{yy} + \varepsilon_{zz}) \quad (15)$$

And the valence bands are shifted by :

$$\delta E_{lh} = a_v.(\varepsilon_{xx} + \varepsilon_{yy} + \varepsilon_{zz}) - \frac{b}{2}.(\varepsilon_{xx} + \varepsilon_{yy} - 2\varepsilon_{zz}) \quad (16)$$

$$\delta E_{hh} = a_v.(\varepsilon_{xx} + \varepsilon_{yy} + \varepsilon_{zz}) + \frac{b}{2}.(\varepsilon_{xx} + \varepsilon_{yy} - 2\varepsilon_{zz}) \quad (17)$$

a_c and a_v are the conduction-band and valence-band hydrostatic deformation potentials, and b is the valence-band shear deformation potential.

For tensile misfit strain, the energy of the bandgap undergoes the fluctuation expressed by the equation 18, while that deformed by compressive strain, is given by equation 19.

$$E_g(Constrained) = \begin{cases} E_{g0} + \delta E_c - \delta E_{lh} & (18) \\ E_{g0} + \delta E_c - \delta E_{hh} & (19) \end{cases}$$

The input simulation data for the different material layers used in the device were meticulously selected from the literature [20-22], ensuring accurate representation of the materials' properties.

3. Methodology

This work is organized as follows. The first step is to describe the structure under study. Next, a detailed simulation model is presented, which accounts for the variation in photovoltaic parameters as a function of the increase in bromine content in the absorber, represented by the ratio x, and the impact of the misfit strain on the energy band edges of the absorber and the performance of the device. This is followed by the calculation stage, where the photovoltaic parameters are evaluated as a function of x, both in the absence of strain and under the influence of the misfit strain. The results are then presented and discussed to highlight the effect of the strain. Based on the adjusted results, the optimal x value for achieving the best conversion efficiency in the strained structure is determined.

3.1 Effects of the Introduction of Bromine on the Perovskite Absorber

The introduction of bromine into the absorber crystal causes a variation in the volume of its unit cell due to the change in the lattice constant [23]. Although the structure of the material remains cubic regardless of the bromine content, the lattice parameter decreases from 6.25 Å to 5.85 Å as the bromine ratio x increases from 0 to 1, as shown in figure 2 a.The different lattice parameters of the $CsSn(I_{1-x}Br_x)_3$ absorber and the SnO_2 electron transport layer generate a misfit strain at the interface between the two layers, which also varies as a function of x. Figure 2 b illustrates that this strain increases from -0.23 to -0.18 as x increases, but remains negative throughout the range of x, indicating a compressive nature of the strain. This compressive strain demonstrates that the absorber is always subjected to compressive deformation to align with the SnO_2 layer. As a result of the misfit strain, the conduction and valence band edges of the $CsSn(I_{1-x}Br_x)_3$ material experience shifts that modify the bandgap energy.

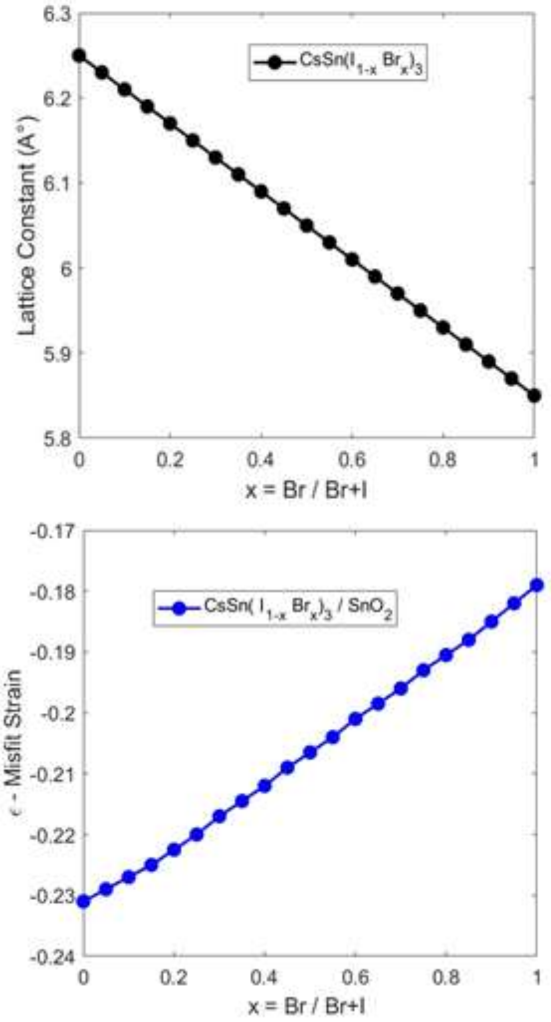

Figure 2. *Variation as a function of x of* ***(a)*** *Lattice constant of* $CsSn(I_{1-x}Br_x)_3$ *and* ***(b)*** *Misfit strain at* $CsSn(I_{1-x}Br_x)_3 /SnO_2$ *interface.*

3.2 Band Edge Shifs and Bandgap Adjustments

The band edge displacements were calculated as a function of x, taking into account the compressive nature of the strain, according to equations 15, 16, and 17. The adjusted bandgap energy is represented in figure.3 and compared with that of the unstrained structure, which neglects the effects of misfit strain. The figure shows that as x increases from 0 to 1, the bandgap energy of the strained $CsSn(I_{1-x}Br_x)_3$ absorber varies from 1.3 eV to 1.82 eV, whereas the bandgap energy of the unstrained structure varies from 1.3 eV to 1.75 eV. This indicates that the presence of misfit strain between the absorber and the ETL results in an increased bandgap energy of the absorber.

The figure also illustrates that the separation between the curves representing the strained and unstrained structures widens as x increases. This widening indicates that the effect of the misfit strain on the bandgap energy becomes more pronounced with higher bromine content. Consequently, all

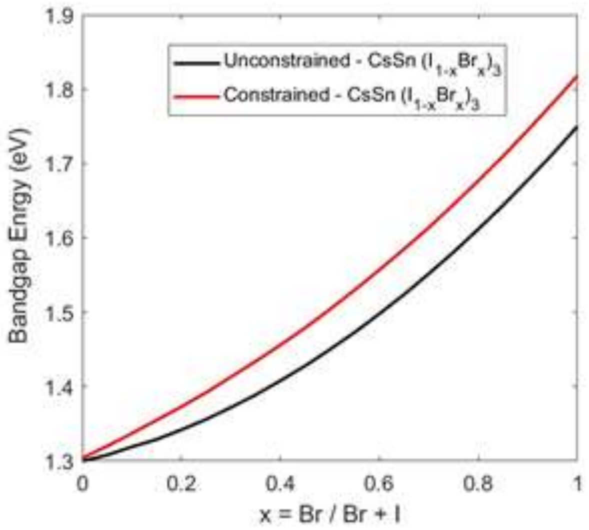

Figure 3. *Bandgap energy of* $CsSn(I_{1-x}Br_x)_3$ *as a function of x-ratio.*

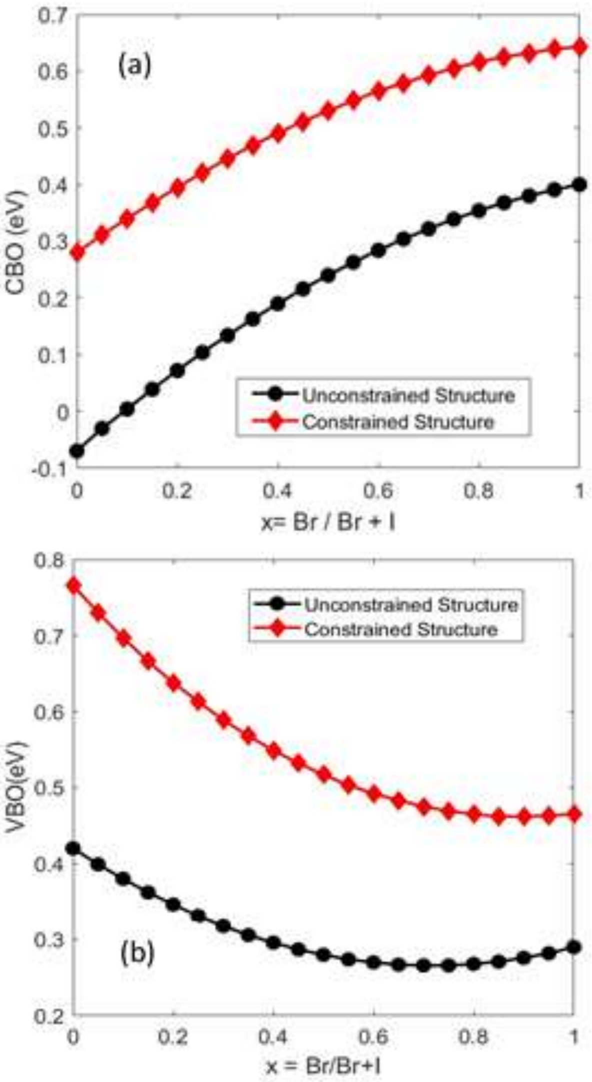

Figure 4.(a) *Conduction band offset at* $CsSn(I_{1-x}Br_x)_3$ / SnO_2 *interface as function of x.* ***(b)*** *Valence band offset at* Cu_2O / $CsSn(I_{1-x}Br_x)_3$ *interface as function of x-ratio.*

photovoltaic parameters are expected to fluctuate due to the strain, as they are intrinsically related to the bandgap energy of the absorber.The conduction and valence band edges at the absorber boundaries with the adjacent ETL and HTL layers will also experience changes due to the displacement of the band edges, as demonstrated in figure 4. Figure 4 (a) shows that when strain is neglected, the conduction band offset CBO is negative, indicating that the energy barrier is cliff-like and increases from -0.07 eV to 0 eV as x changes from 0 to 0.1. When x increases from 0.1 to 1, the CBO becomes positive, which means the energy barrier takes the form of a spike and rises to 0.4 eV. In this case, the conduction band shift is favorable across the entire range of x. However, when strain is considered, the CBO increases from 0.34 eV to 0.64 eV, remaining positive as x varies from 0 to 1. This indicates that the energy barrier in this scenario is also spike-like, with a favorable effect only between x = 0 and x = 0.35. A similar behavior is observed for the variation of the valence band offset VBO as a function of x. When strain is neglected, the VBO decreases from 0.42 eV to 0.29 eV. In contrast, when strain is taken into account, the VBO becomes more significant, decreasing from 0.76 eV to 0.47 eV.

3.3 Impact of Misfit Strain on Photovoltaic Parameters

The photovoltaic parameters of the device are influenced by fluctuations in the band gap energy due to misfit strain at the front interface. Figure 5 illustrates the variation in the cell's electrical parameters as a function of x in two scenarios: considering the strain and neglecting the strain between the absorber and the ETL layer. All the figures confirm the fluctuation of the photovoltaic parameters due to misfit strain. The behavior of the open-circuit voltage and the fill factor in figure 5(b) and (c) mirrors that of the bandgap energy shown in figure 3. Concerning the photocurrent density and conversion efficiency shown in figure 5(a) and figure 5(d), the difference between the strained and unstrained cases is negligible at low bromine contents but becomes noticeable above x = 0.15. Figure 5(a) and figure (d) also illustrate that photocurrent density and conversion efficiency initially increase with x, reach a maximum, and then decrease. This is attributed to the increasing trap defect density as bromine, which has a larger volume than iodine, is introduced into the absorber’s composition, causing structural disorder. A maximum efficiency of 19.72% is observed at x = 0.56 for the unstrained structure, and 19.3% at a slightly lower bromine content, x = 0.5, for the strained structure. The corresponding voltage-current characteristics for the unstrained case at x = 0.56 and the strained case at x = 0.56 are shown in figure 6.

4. Simulation Results and Analysis of Performance Compared to Similar Structures

The numerical results for the photovoltaic parameters are summarized in table 1. and compared with those from perovskite solar cell structures that use similar absorbers, with or without lead. When

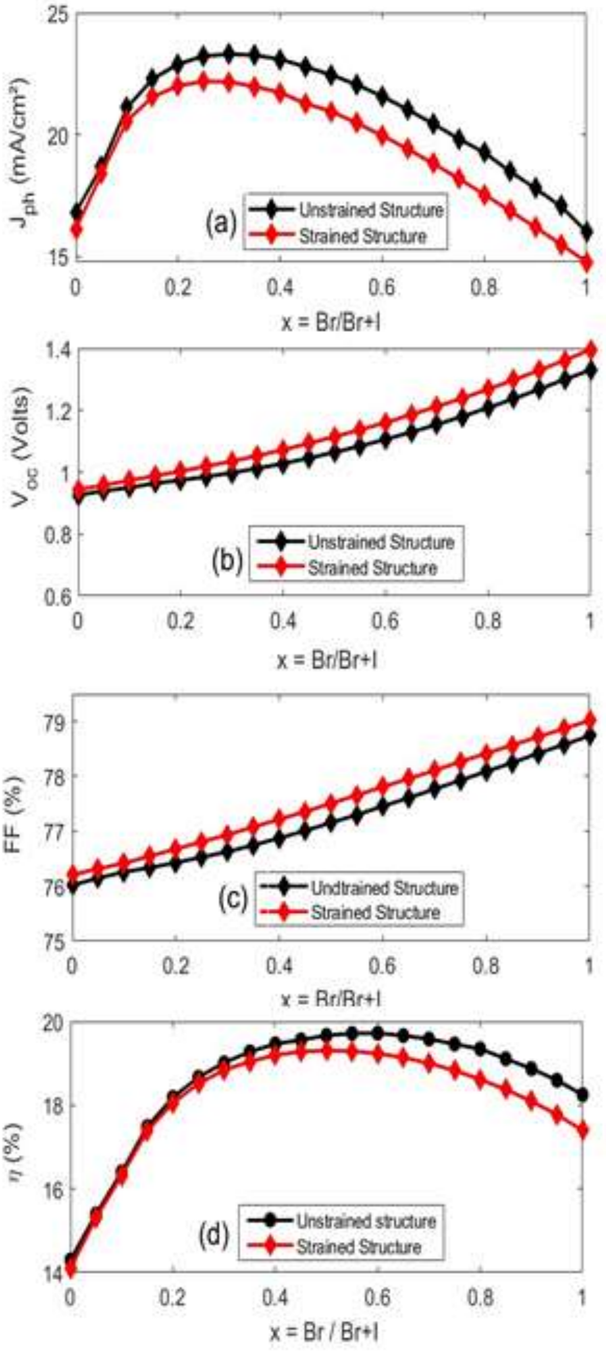

Figure 5. *Photovoltaic performance of strained and unstrained* $CsSn(I_{1-x}Br_x)_3/SnO_2$*-based solar cells as a function of the x-ratio.*

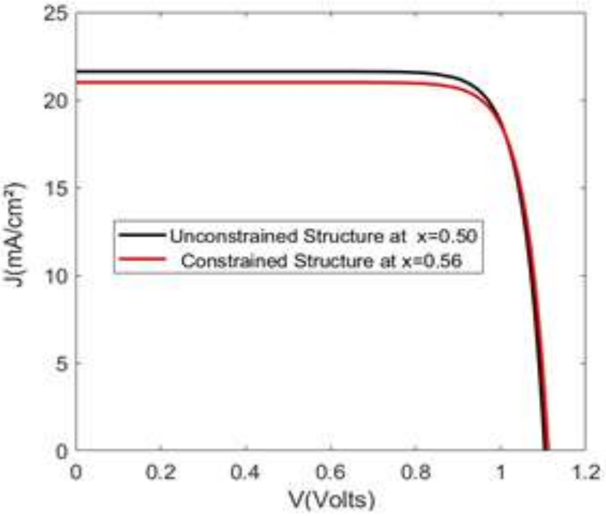

Figure 6. *J-V characteristics of unconstrained and constrained device structures.*

compared to the lead-based inorganic or hybrid perovskite structures reported in [24-25], which have a comparable bandgap to that of the studied absorber, the photovoltaic parameters are found to be very similar.However, while the conversion efficiency of the simulated structure is favorable, it is slightly less than that of the reported structures, regardless of strain conditions.

Nevertheless, the simulated structure's advantages include being fully inorganic, offering greater stability compared to structures with organic or hybrid absorbers, and being lead-free, which ensures it is non-toxic.

5. Conclusion

In this work, we studied the performance of a single solar cell based on the perovskite absorber material configured as SnO_2 / $CsSn(I_{1-x}Br_x)_3$ / Cu_2O. The absorber material is a lead-free, inorganic perovskite with a variable composition determined by the bromine content, represented by the x-ratio. The electron and hole transport layers, SnO_2 and Cu_2O, were carefully selected based on prior research. Our simulation model incorporates the variation of physical parameters of the perovskite absorber as a function of composition, allowing for the calculation of J-V characteristics and photovoltaic parameters with these variations.

Table1*. Simulation Results*

Structure	**Br/Br+I**	**E_g (eV)**	**J_{ph} (mA/cm^2)**	**V_{oc} (V)**	**FF (%)**	**PCE (%)**
Unstrained $CsSn(I_{1-x}Br_x)_3$	0.56	1.48	22.00	1.10	77.3	19.71
Strained $CsSn(I_{1-x}Br_x)_3$	0.50	1.50	21.00	1.11	77.5	19.31
$MAPb(I_{1-x}Br_x)_3$ Cell [24]	/	1.61	20.65	1.18	86.5	21.21
$CsPb(I_{1-x}Br_x)_3$ Cell-Sim [25]	/		21.61	1.25	78.13	21.18
$CsPb(I_{1-x}Br_x)_3$ Cell-exp [25]	/	1.65	20.70	1.25	86.5	21.14

The study also addresses the impact of misfit strain due to the lattice mismatch between the absorber and the ETL layer at the front interface on the fluctuation of energy band edges. We introduced strain theory calculations into the simulation model to account for the shifts in conduction and valence band energies. By comparing the photovoltaic parameters of the structure under both strained and unstrained conditions, we demonstrated the importance of considering misfit strain for accurately determining the optimal bromine content to achieve maximum efficiency. The results revealed a maximum efficiency of 19.72% at x = 0.56 for the unstrained structure and 19.30% at x = 0.50 for the strained structure. This study offers valuable insights, highlighting that misfit strain can be a useful tool for tuning the bandgap energy in addition to adjusting the composition for improved solar cell performance. Solar cell is well studied in past and reported some results [26-29].

Author Statements:

- **Ethical approval:** The conducted research is not related to either human or animal use.
- **Conflict of interest:** The authors declare that they have no known competing financial interests or personal relationships that could have appeared to influence the work reported in this paper
- **Acknowledgement:** The authors declare that they have nobody or no-company to acknowledge.
- **Author contributions:** The authors declare that they have equal right on this paper.
- **Funding information:** The authors declare that there is no funding to be acknowledged.
- **Data availability statement:** The data that support the findings of this study are available on request from the corresponding author. The data are not publicly available due to privacy or ethical restrictions.

References

[1] Dada, M., & Popoola, P. (2023). Recent advances in solar photovoltaic materials and systems for energy storage applications: A review. *Beni-Suef University Journal of Basic and Applied Sciences, 12*(1), 66. https://doi.org/10.1186/s43088-023-00405-5

[2] Arbouz, H. (2022). Modeling of a tandem solar cell structure based on CZTS and CZTSe absorber materials. *International Journal of Computational and Experimental Science and Engineering, 8*(1), 14-18. https://doi.org/10.22399/ijcesen.843038

[3] Gressler, S., Part, F., Scherhaufer, S., Obersteiner, G., & Huber-Humer, M. (2022). Advanced materials for emerging photovoltaic systems – Environmental hotspots in the production and end-of-life phase of organic, dye-sensitized, perovskite, and quantum dots solar cells. *Sustainable Materials and Technologies, 34*, e00501. https://doi.org/10.1016/j.susmat.2022.e00501

[4] Fouladi Targhi, F., Seyed Jalili, Y., & Kanjouri, F. (2018). MAPbI3 and FAPbI3 perovskites as solar cells: Case study on structural, electrical, and optical properties. *Results in Physics, 10*, 616-627. https://doi.org/10.1016/j.rinp.2018.07.007

[5] Costa, C., Manceau, M., Duzellier, S., Nuns, T., & Cariou, R. (2023). Perovskite solar cells under protons irradiation: From in-situ IV-monitoring to root cause degradation elucidation. *Solar Energy Materials and Solar Cells, 257*, 112388. https://doi.org/10.1016/j.solmat.2023.112388

[6] Feng, J., Wang, X., Li, J., Zhang, X., & Zhao, L. (2023). Resonant perovskite solar cells with extended band edge. *Nature Communications, 14*(1), 5392. https://doi.org/10.1038/s41467-023-41149-1

[7] Arbouz, H. (2023). Optimization of lead-free CsSnI3-based perovskite solar cell structure. *Applied Rheology, 33*(1), 20220138. https://doi.org/10.1515/arh-2022-0138

[8] Arbouz, H. (2022). Simulation and optimization of a lead-free CS2TiBr6 perovskite solar cell structure. In *Proceedings of International Conference on Electrical Computer Communications and Mechatronics Engineering* (pp. 1-6). IEEE.

[9] Arbouz, H. (2023). Towards efficient tandem solar cells based on lead-free and inorganic perovskite absorbers. *Thermal Science and Engineering, 6*(1), 34. https://doi.org/10.24294/tse.v6i1.2000

[10] Arbouz, H. (2023). Simulation and optimization of a solar cell based on the double perovskite absorber material Cs2BiAgI6. In *Proceedings of the 3rd International Conference on Electrical, Computer, Communications and Mechatronics Engineering (ICECCME)* (pp. 1-6). IEEE. https://doi.org/10.1109/ICECCME57830.2023.10252226

[11] Bin, W.-M., Huang, W.-H., Lin, W.-C., & Lee, H. (2021). Study on optical and electrical properties of thermally evaporated tin oxide thin films for perovskite solar cells. *Crystals, 11*(11), 1380. https://doi.org/10.3390/cryst11111380

[12] Katariya, A., Mahapatra, B., Patel, P., & Rani, J. (2021). Optimization of ETM and HTM layer on NFA based BHJ-organic solar cell for high efficiency performance. *Optik, 245*, 167717. https://doi.org/10.1016/j.ijleo.2021.167717

[13] Arbouz, H. (2023). Simulation study of single solar cell structures based on the compositionally variable perovskite material CsSn(I1-xBrx)3 for tandem configured solar cells. *Journal of Engineering Research*. https://doi.org/10.1016/j.jer.2023.09.030

[14] Ghosh, R., Singh, A., & Agarwal, P. (2023). Study on the effect of different HTL and ETL materials on the perovskite solar cell performance with TCAD simulator. *Materials Today: Proceedings*. https://doi.org/10.1016/j.matpr.2023.06.161

[15] Rawa, M., Al-Turki, Y., Sindi, H., Ćalasan, M., Ali, Z. M., & Abdel Aleem, S. H. E. (2023). Current-voltage curves of planar heterojunction perovskite solar cells – Novel expressions based on Lambert W function and Special Trans Function Theory. *Journal of Advanced Research, 44*, 91-108. https://doi.org/10.1016/j.jare.2022.03.017

[16] Courel, M., Andrade-Arvizu, J. A., & Vigil-Galán, O. (2014). Towards a CdS/Cu2ZnSnS4 solar cell efficiency improvement: A theoretical approach. *Applied Physics Letters, 105*(23), 233501. https://doi.org/10.1063/1.4903826

[17] Ghobadi, A., Yousefi, M., Minbashi, M., Ahmadkhan Kordbacheh, A. H., Haji Abdolvahab, A. R., & Gorji, N. E. (2020). Simulating the effect of adding BSF layers on Cu2BaSnSSe3 thin film solar cells. *Optical Materials, 107*, 109927. https://doi.org/10.1016/j.optmat.2020.109927

[18] Zhang, P., Song, Y., Tian, J., Zhang, X., & Zhang, Z. (2009). Gain characteristics of the InGaAs strained quantum wells with GaAs, AlGaAs, and GaAsP barriers in vertical-external-cavity surface-emitting lasers. *Journal of Applied Physics, 105*(5), 053103. https://doi.org/10.1063/1.3081558

[19] Van de Walle, C. G. (1989). Band lineups and deformation potentials in the model-solid theory. *Physical Review B: Condensed Matter, 39*(3), 1871-1883. https://doi.org/10.1103/PhysRevB.39.1871

[20] Hossain, M. K., Toki, G. F. I., Kuddus, A., Uddin, M. S., & Islam, M. R. (2023). An extensive study on multiple ETL and HTL layers to design and simulation of high-performance lead-free CsSnCl3-based perovskite solar cells. *Scientific Reports, 13*(1), 2521. https://doi.org/10.1038/s41598-023-28506-2

[21] Sidra, K., Yadav, S., Chakraborty, V., Singh, J., & Singh, R. (2023). A simulation study of all inorganic lead-free CsSnBr3 tin halide perovskite solar cell. *Materials Today: Proceedings*. https://doi.org/10.1016/j.matpr.2023.04.167

[22] Hossain, M. K., Uddin, M. S., Toki, G. F. I., Mohammed, M. K. A., Pandey, R., Madan, J., Rahman, M. F., Islam, M. R., Bhattarai, S., Bencherif, H., Samajdar, D. P., Amami, M., & Dwivedi, D. K. (2023). Achieving above 24% efficiency with non-toxic CsSnI3 perovskite solar cells by harnessing the potential of the absorber and charge transport layers. *RSC Advances, 13*(34), 23514-23537. https://doi.org/10.1039/d3ra02910g

[23] Zhu, C., Niu, X., Fu, Y., Wang, Q., & Zhang, H. (2019). Strain engineering in perovskite solar cells and its impacts on carrier dynamics. *Nature Communications*, *10*(1), 815. https://doi.org/10.1038/s41467-019-08507-4

[24] Ahmed, A., Riaz, K., Mehmood, H., Tauqeer, T., & Ahmad, Z. (2020). Performance optimization of CH3NH3Pb(I1-xBrx)3 based perovskite solar cells by comparing different ETL materials through conduction band offset engineering. *Optical Materials*, *105*, 109897. https://doi.org/10.1016/j.optmat.2020.109897

[25] Wang, L., Yang, S., Xi, T., Yang, Q., Yi, J., Li, H., & Zhong, J. (2023). Performance optimization of CsPb(I1–xBrx)3 inorganic perovskite solar cells with gradient bandgap. *Energies*, *16*(10), 4135. https://doi.org/10.3390/en16104135

[26] Demirhan, Y. (2024). Multi-Layer Absorber based on Plasmonic Resonances for Photovoltaic Applications at Visible Spectra. *International Journal of Computational and Experimental Science and Engineering*, 10(4);1712-1718. https://doi.org/10.22399/ijcesen.778

[27] Polatoglu, A. (2024). Observation of the Long-Term Relationship Between Cosmic Rays and Solar Activity Parameters and Analysis of Cosmic Ray Data with Machine Learning. *International Journal of Computational and Experimental Science and Engineering*, 10(2);189-199. https://doi.org/10.22399/ijcesen.324

[28] ABDELBAKI , C., & REBIHA , L. (2015). Modeling of silicon solar cells performances by MATLAB. *International Journal of Computational and Experimental Science and Engineering*, 1(1), 11–15. Retrieved from https://www.ijcesen.com/index.php/ijcesen/article/view/12

[29] Arbouz, H. (2024). Study of an Efficient and Environmentally Friendly Germanium-Based CsGeI3 Perovskite Structure For Single and Double Solar Cells . *International Journal of Computational and Experimental Science and Engineering*, 10(1);33-41. https://doi.org/10.22399/ijcesen.250